BIOCHEMISTRY

 Volume 44, Number 33 August 23, 2005

Accelerated Publications

Structural Characterization of a Complex of Photosystem I and Light-Harvesting Complex II of *Arabidopsis thaliana*†

Roman Kouřil,‡ Agnieszka Zygadlo,§ Ana A. Arteni,‡ Chantal D. de Wit,|| Jan P. Dekker,|| Poul Erik Jensen,§ Henrik Vibe Scheller,§ and Egbert J. Boekema*,‡

Department of Biophysical Chemistry, GBB, University of Groningen, Nijenborgh 4, 9747 AG Groningen, The Netherlands, Plant Biology Laboratory, Department of Plant Biology, The Royal Veterinary and Agricultural University, 40 Thorvaldsenvej, Frederiksberg C, DK-1871, Denmark, and Division of Physics and Astronomy, Faculty of Sciences, Vrije Universiteit, De Boelelaan 1081, 1081 HV Amsterdam, The Netherlands

Received June 9, 2005; Revised Manuscript Received July 4, 2005

ABSTRACT: Chloroplasts are central to the provision of energy for green plants. Their photosynthetic membrane consists of two major complexes converting sunlight: photosystem I (PSI) and photosystem II (PSII). The energy flow toward both photosystems is regulated by light-harvesting complex II (LHCII), which after phosphorylation can move from PSII to PSI in the so-called state 1 to state 2 transition and can move back to PSII after dephosphorylation. To investigate the changes of PSI and PSII during state transitions, we studied the structures and frequencies of all major membrane complexes from *Arabidopsis thaliana* chloroplasts at conditions favoring either state 1 or state 2. We solubilized thylakoid membranes with digitonin and analyzed the complete set of complexes immediately after solubilization by electron microscopy and image analysis. Classification indicated the presence of a PSI−LHCII supercomplex consisting of one PSI−LHCI complex and one LHCII trimer, which was more abundant in state 2 conditions. The presence of LHCII was confirmed by excitation spectra of the PSI emission of membranes in state 1 or state 2. The PSI−LHCII complex could be averaged with a resolution of 16 Å, showing that LHCII has a specific binding site at the PSI-A, -H, -L, and -K subunits.

Oxygenic photosynthesis relies on a balanced system of light harvesting and the conversion of the light energy into chemical energy in the photosynthetic reaction centers of PSI[1] and PSII. PSI and PSII have different absorption spectra. The light energy fluctuates in intensity and quality, and plants can adapt to the changing light conditions by directing the absorbed light to either PSI or PSII to keep the energy conversion efficient. The response of the photosynthetic apparatus to light fluctuations is called state transitions (*1*−*3*). State transitions occur in three main steps. Upon preferential excitation of PSII, the linear electron flow between PSI and PSII may become unbalanced, resulting in an over-reduction of the plastoquinone (PQ) pool and the

† R.K., A.Z., and the groups of H.V.S., J.P.D., and E.J.B. were supported by the European Union, Grant HPRN-CT-2002-00248 ("PSICO network"); E.J.B was also supported by The Netherlands Organisation for Scientific Research, Council for Earth and Life Sciences. C.D.W. was supported by The Netherlands Foundation for Fundamental Research on Matter.

* To whom correspondence should be addressed. Tel. +31 50 3634225; fax, +31 50 3634800; e-mail, e.j.boekema@rug.nl.

‡ University of Groningen.

§ The Royal Veterinary and Agricultural University.

|| Vrije Universiteit.

[1] Abbreviations: LHCI, light-harvesting complex I; LHCII, light-harvesting complex II; PSI, photosystem I; PSII, photosystem II.

10.1021/bi051097a CCC: $30.25
Published on Web 07/28/2005

cytochrome b_6f complex (*4*, *5*). The first step is the initiation of a signal transduction, brought about by reduced state of the PQ pool and the cytochrome b_6f complex, leading to the activation of kinases. The second step is the phosphorylation, by the activated kinases, of the mobile PSII antenna, the light-harvesting complex II (LHCII). In plants, the major LHCII proteins consist of three closely related chlorophyll *a*/*b*-binding proteins encoded by *Lhcb1*, *Lhcb2*, and *Lhcb3* genes (*6*). However, it remains uncertain whether the mobile LHCII consists of a monomer or a trimer of lhcb proteins. Two kinase families are proposed to be involved in LHCII phosphorylation: TAK kinases (*7*, *8*) and STT7 kinases in *Chlamydomonas* (*9*) and its homologue in *Arabidopsis* STN7 (*10*). The corresponding mutants of those kinases cannot perform phosphorylation of LHCII and state transitions. The phosphorylation of LHCII is thought to cause a conformational change, which allows LHCII to diffuse to PSI in the thylakoid membrane, constituting the last step in state transitions (*1*). The binding of phosphorylated LHCII to PSI brings the system in state 2 and allows a redistribution of the light energy between the two photosystems and a balancing of the linear electron flow. This association between PSI and LHCII is reversible. Preferential excitation of PSI leads to oxidation of the plastoquinol pool, a dephosphorylation of LHCII, and a release of LHCII from the PSI−LHCII complex (state 1).

There are recent data indicating which PSI subunits play an essential role in the state transitions. *Arabidopsis* plants without the PSI-H and PSI-L subunits (*11*), as well as those without the PSI-O subunit (*12*), are highly deficient in state transitions. Chemical cross-linking using dithio-bis(succinimidylpropionate) followed by diagonal electrophoresis and immunoblotting showed that the docking site of LHCII on PSI is comprised of the PSI-H, -L, and -I subunits (*13*). Thus, despite ample evidence for a functional interaction between LHCII and PSI, direct evidence for the existence of a physical complex between the two and the precise docking site of LHCII on PSI has not been demonstrated. Another open question is the origin of LHCII which associates to PSI. LHCII is mainly organized as trimers, and the usual ratio of LHCII trimers to dimeric PSII core complexes is about 8:1. In *Arabidopsis*, most PSII core complexes bind only 2−4 LHCII trimers, which implies a pool of nonbound or very loosely bound LHCII (*14*). Thus, the LHCII which associates to PSI can originate either from the nonbound LHCII pool or from PSII−LHCII supercomplexes. A further question deals with the association state of the LHCII proteins binding to PSI. Binding of phosphorylated LHCII monomers to PSI has been suggested (*1*, *8*), but more recent work shows that phosphorylation is not a prerequisite for binding to PSI (*13*).

Structural studies usually require purified proteins. The purification of a PSI−LHCII supercomplex after digitonin solubilization of *Arabidopsis* membranes was recently described (*13*). However, these PSI−LHCII supercomplexes appeared to be too fragile to obtain in sufficient quantity for structural analysis. Single-particle electron microscopy is an effective method for both the sorting and averaging of molecular projections of large membrane proteins. We have previously shown that this technique can be used to analyze the composition of PSII−LHCII supercomplexes in partially solubilized grana membranes immediately after solubilization and without any purification (*15*). Hence, we have performed an analysis of all possible PSI and PSII projections from *Arabidopsis* thylakoid membranes of chloroplasts, brought either in state 1 or state 2 before they were solubilized with digitonin. Analysis of the set of single-particle projections reveals for the first time a supercomplex consisting of one PSI complex and one trimeric LHCII, which is more abundant in state 2. The projection map could be resolved at 16 Å resolution, which reveals the precise position of LHCII.

MATERIALS AND METHODS

Plant Material and Growth Conditions. Arabidopsis thaliana (L.) Heynh. ecotype Columbia was used for all experiments. Plants were grown in compost in a controlled environment Arabidopsis Chamber (Percival AR-60L, Boone, IA) at a photosynthetic flux of 100−120 μmol photons m^{-2} s^{-1}, 20 °C, and 70% relative humidity. The photoperiod was 8 h to suppress the induction of flowering.

Induction of State Transitions. Four-to-six week-old plants were used for light treatment. An orange filter (Rosco, 105 orange, Teadan Aps, Stenløse, Denmark) adjusted with a gray filter (209 neutral density, LEE Filters, Andover, U.K.) to 70 μmol photons m^{-2} s^{-1} was used to induce state 2 in plants, and a red filter (HT 027 medium red, LEE Filters) adjusted with gray filters to 50 μmol photons m^{-2} s^{-1} was used to induce state 1. The filters were mounted in a controlled environment chamber equipped with 400-watt Powertone HPI-T Plus lamp (Philips). Plants were exposed to state 1 or state 2 light for 1 h; leaves were harvested under state 1 or state 2 light and immediately frozen in liquid nitrogen. We have previously shown that this light treatment induces state transitions efficiently (*13*).

Isolation of Thylakoid Membranes. Leaves from light-treated plants were used for isolation of thylakoids as described previously (*16*). Total chlorophyll and chlorophyll *a*/*b* ratio in thylakoids were determined in 80% acetone according to ref *17*. The 77 K fluorescence emission spectra were recorded of the thylakoid preparations from state 1 and state 2 to verify that the light treatment induced state transitions in the plants.

Solubilization of Thylakoid Membranes. Thylakoid membranes were resuspended in 20 mM Bis-Tris (pH 6.5) with 5 mM $MgCl_2$ at a final concentration of 0.5 mg of Chl/mL and solubilized with digitonin at a final concentration of 0.5% (w/v) for 30 min at 4 °C with stirring according to ref *13*, followed by centrifugation in an Eppendorf table centrifuge for 15−20 min. The entire solubilized sample was directly used for preparation of specimen for electron microscopy without any purification step.

Fluorescence Measurements. For the low-temperature, steady-state fluorescence measurements, the membranes were diluted in a buffer containing 20 mM Bis-Tris, pH 6.5, 20 mM NaCl, 5 mM $MgCl_2$, and 66% (v/v) glycerol as a cryoprotectant. The final optical density of the membranes was less than 0.1 cm^{-1} at 680 nm.

Fluorescence emission spectra were measured with a 0.5 m imaging spectrograph (Chromex 500IS) and a CCD camera (Chromex Chromcam I). The spectral resolution was 0.15 nm. For broadband excitation, a tungsten halogen lamp (Oriel) was used with an interference filter transmitting at 420 nm, bandwidth 15 nm. A helium bath cryostat (Utreks,

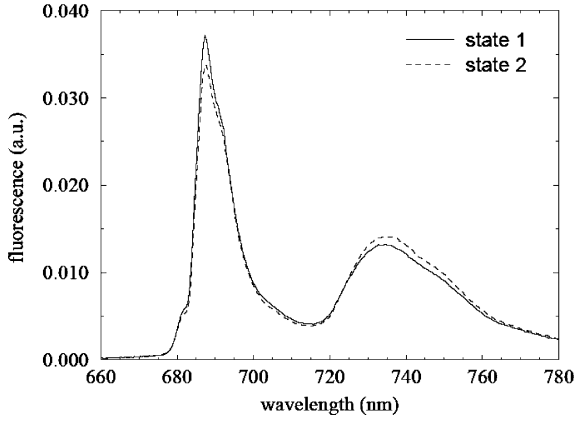

FIGURE 1: The 5 K fluorescence emission spectra of *Arabidopsis thaliana* membranes in state 1 and state 2 following 420 nm excitation. The spectra were scaled to unity total fluorescence emission yield.

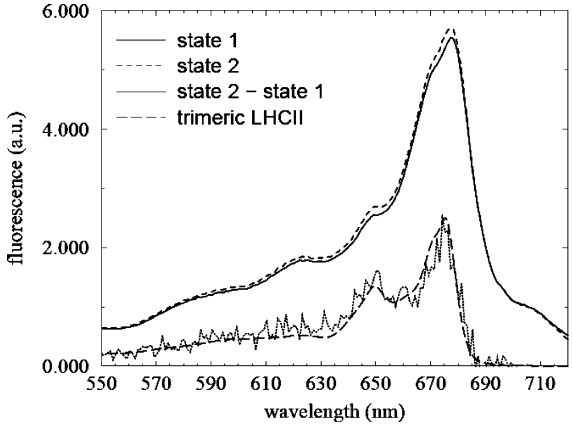

FIGURE 2: The 77 K fluorescence excitation spectra of *Arabidopsis thaliana* membranes both in state 1 and state 2, recorded at 735 nm. The spectra were normalized to the red pigments absorbing around 705 nm, thus, assuming conservation of PSI upon state transitions. Shown is their difference spectrum and the fluorescence excitation spectrum of trimeric LHCII.

4 K) was used to cool the samples. Fluorescence excitation spectra were measured with a fluorimeter (Jobin Yvon, FL, *3*−*11*). The membranes were excited by a tungsten halogen lamp, with both excitation and detection bandwidth 2 nm. The fluorescence was detected at 735 nm. A nitrogen cryostat (Oxford) was used to cool the samples to 77 K.

Electron Microscopy and Single-Particle Analysis. Samples were negatively stained using the droplet method with 2% uranyl acetate on glow-discharged, carbon-coated copper grids. Electron microscopy was performed on a Philips CM20 FEG electron microscope operated at 200 kV. Images were recorded with a Gatan 4000 SP 4K slow-scan camera at 66 850× magnification with a pixel size (after binning the images) of 4.49 Å at the specimen level, with "GRACE" software for semi-automated specimen selection and data acquisition. A total of 4200 images was recorded from three different samples of purified complexes from state 1 and 2 membranes each. Single-particle analysis was performed with the Groningen Image Processing ("GRIP") software package on a PC cluster. Selected single-particle projections (128 × 128 pixel frame) were aligned by a multireference alignment and reference-free alignment procedures (*18*, *19*). Then, particles were subjected to multivariate statistical analysis, followed by hierarchical ascendant classification (HAC) (*19*). The resolution of the class averages was measured by Fourier Ring Correlation according to ref *20*. Truncated versions and 2D projection maps of X-ray structures of PSI (*24*) and LHCII (*25*, *26*) at 15 Å resolution were generated using routines from the EMAN package (*27*). Surface representations of the truncated structures were generated with VIS5D software (www.ssec.wisc.edu/∼billh/vis5d.html) and manually superimposed on averaged projections of the PSI−LHCII complex.

RESULTS

Characterization of Membranes in State 1 and State 2. We prepared *Arabidopsis* membranes in state 1 or state 2 by red or orange light treatment as described previously (*13*). Figure 1 displays fluorescence emission spectra at 5 K of the state 1 and state 2 membranes upon 420 nm excitation. The spectra indicate that, upon going from state 1 to state 2, the emission of PSI at 735 nm increases, the emission of PSII at 687 and 692 nm decreases, and the emission of uncoupled LHCII at 682 nm does not change significantly. Figure 2 shows 77 K fluorescence excitation spectra at 735 nm of the state 1 and state 2 membranes, normalized to the content of red pigments around 705 nm. The membranes in state 2 receive more excitation energy from chlorophylls absorbing around 675 and 650 nm, and the fluorescence excitation difference spectrum (dotted line) resembles the excitation spectrum of trimeric LHCII (long dashes). This indicates that the PSI light-harvesting antenna is extended with LHCII upon a transition to state 2.

Electron Microscopy of Digitonin-Solubilized Membranes. Electron micrographs of digitonin-solubilized thylakoid membranes revealed the presence of projection views of all the major membrane proteins, including photosystems I and II and the F_0F_1 ATPase complex (Figure 3). Sets of about 11 000 and 15 000 projections were selected from digitonin-solubilized membranes prepared in state 1 and state 2, respectively. We picked all projections with the size of tentative PSI particles (*21*) and all PSII projections larger than or similar to a C_2S_2 PSII−LHCII supercomplex (*22*). The PSI and PSII projections comprised about 80% and 20% of the selected data set, respectively. The state 1 and state 2 and the PSI and PSII projections, were separately processed, and final results from statistical analysis and classification are presented in Figure 4. The majority of projections of PSI in state 2 represent either the oval shaped PSI−LHCI complex (Figure 4D) or a novel pear-shaped particle, representing a supercomplex between PSI and trimeric LHCII (discussed below). This pear-shaped particle is represented by three class-averages (Figure 4A−C). The image of Figure 4A represents a particle which is 25% larger in projection than PSI. The surface of the other two class-sums is slightly smaller; it appears that some density is reduced at the upper-left side (Figure 4, arrowheads). The same projections were obtained from state 1 membranes, but with the pear-shaped particles in much smaller numbers. However, the overall quality of state 1 images is a bit lower, and projections appear more blurred. This complicated the alignment and classification procedure of half of the set, not in the least because the oval-shaped PSI projections are rather featureless, in contrast to the rectangular PSII projections with a favorable staining of the extrinsic subunits. About half of the particles were intermediate in size between PSI and PSI−LHCII. A sum

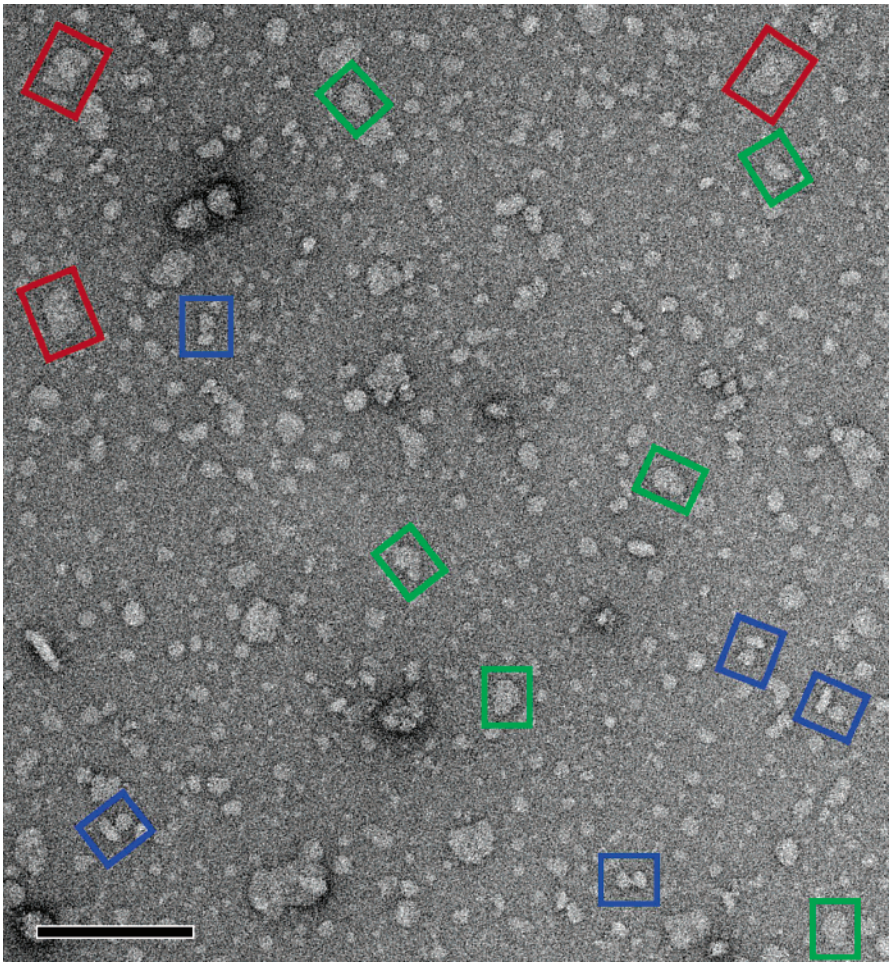

FIGURE 3: Part of an electron micrograph of nonpurified single particles from digitonin solubilized thylakoid membranes of *Arabidopsis thaliana* in state 2. Projections of PSI/PSI−LHCII, PSII, and ATP-ases are indicated by green, red, and blue boxes, respectively. The scale bar equals 100 nm.

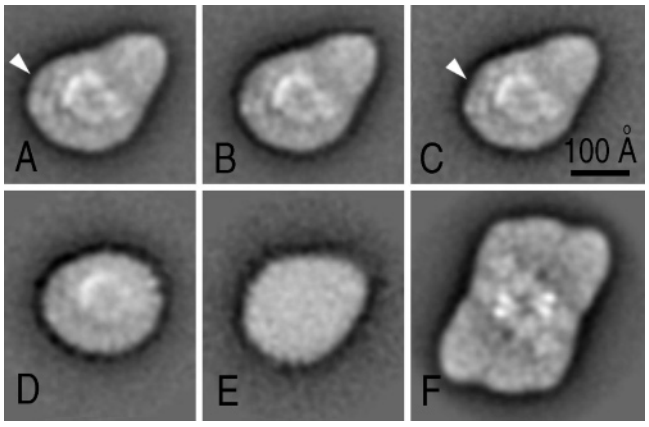

FIGURE 4: Results from single particle electron microscopy. Averaged images represent class-sums of 728 (A), 768 (B), 437 (C), 479 (D), 416 (E), and 300 (F) aligned projections, respectively. The white arrowheads point to a small protein density which is reduced in frames B and C. All projections were from particles extracted from state 2 membranes, except for frame E.

obtained after nonreference alignment indicates a circumference reminiscent of the other two particle types (Figure 4E), but without clear features.

Much lower numbers of PSII supercomplexes were obtained, also because part of the grana membranes remained intact under the applied solubilization conditions. The PSII supercomplex projections are however rather easy to process, and the larger ones could be classified and averaged straightforwardly. The most common particle projection was the $C_2S_2M_2$ supercomplex (Figure 4F); two other types of particles were the smaller C_2S_2M and C_2S_2 supercomplexes. These three particles were identical to PSII complexes from *Arabidopsis*, analyzed previously (*14*, *23*). In the state 2 membranes, the relative number of the smaller C_2S_2M supercomplex was slightly higher (Table 1).

DISCUSSION

Characterization of the PSI−LHCII Complex. For an assignment of the novel pear-shaped PSI−LHCII particle, we compared our final map at 16 Å resolution (Figure 5A) with 2D projection maps and truncated 3D models derived from the atomic models of PSI (*24*) and LHCII (*25*, *26*) (Figure 5B,C). This indicates that we can unambiguously assign our projection map with an association of PSI and trimeric LHCII, as presented in Figure 5C. In the PSI part of our electron microscopy map, the central ridge of the PsaC, -D, and -E subunits, is prominent as the most stain-excluding densities. Interestingly, components of the peripheral antenna are also recognizable. At 15 Å resolution, the EM map and the generated 2D projection map show that especially Lhca1 is well-resolved. Its position is represented by three densities (asterisks in Figure 5A−C). The EM map also shows that the Lhca2 and Lhca3 subunits do not have pronounced features at this resolution, in agreement with the

Table 1: Statistics of Image Analysis and the Relative Numbers of Assigned PSI and PSII Projections[a]

	PSI				PSII			
	number of particles analyzed	percentage projections			number of particles analyzed	percentage projections		
		PSI	PSI−LHCII	blurred		$C_2S_2M_2$	C_2S_2M	C_2S_2
state 1	9530	44	3	53	1500	84	8	8
state 2	11900	42	49	9	3200	68	23	9

[a] Nonassigned "blurred" projections are grouped under the PSI projections.

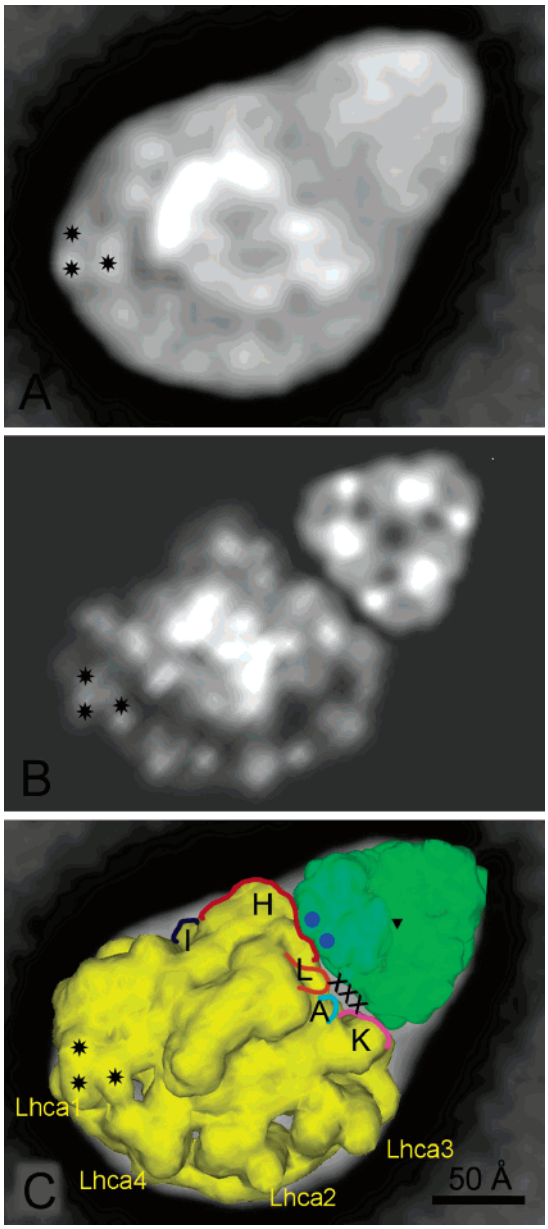

FIGURE 5: (A) Final projection map of the PSI−LHCII supercomplex at 16 Å. (B) Generated 2D projection map of the PSI−LHCII supercomplex from atomic models at 15 Å resolution. (C) Assignment of the supercomplex by fitting of the high-resolution structures of PSI (yellow) and trimeric LHCII (green). One LHCII monomer is indicated in blue-green, blue dots mark the spots where the ends of the helices A and B are closest to PSI in projection, and the center of the trimer is indicated by a triangle. Three densities belonging to Lhca1 are indicated by asterisks in A−C. The surface of subunits PSI-A, -H, -I, -K, and -L closest to the trimer has been indicated. An open space in the interfaces of PSI and LHCII is marked by crosses.

truncated X-ray projection map. The map furthermore indicates that the slight variation between the classes of Figure 4A−C is around the position of subunit PsaG (Figure 5B,C). The LHCII trimer is attached at a defined position between subunits PSI-A, -H, -L, and -K (Figure 5C) and confirms the role of PSI-H and PSI-L in the binding pocket (*13*) and thus in the mechanism of the state transitions. The trimer also interacts with PSI-K, but not with PsaI, although this subunit has been found to cross-link to LHCII (*13*). Modeling of the truncated LHCII trimer furthermore indicates how two of its monomers are in direct contact with the PSI complex.

The involvement of PSI-H and PSI-L in the binding of LHCII is expected in view of the role of these subunits in the state transitions (*11*) and of the detected cross-link to LHCII (*13*). The involvement of PSI-K in the binding of LHCII is however surprising, because the absence of PSI-K by the addition of an antisense construct does not impair state transitions (*28*) and a cross-link between PSI-K and LHCII was not detected (*13*). The absence of PSI-K even resulted in an slightly enhanced binding of LHCII (*13*), which can be explained by a small shift of LHCII toward PSI-A. This is possible because in the presence of PSI-K there seems to be a small gap between PSI-A and LHCII (indicated as XXX in Figure 5C).

Figure 5C shows that the observed cross-link between PSI-I and LHCII (*13*) is hard to explain by the structure of the current PSI−LHCII complex. It is possible though that there is a second binding site of LHCII, which is even weaker than the first and therefore can be missed in our analysis. Cross-linking will prevent the detachment of the cross-linked complex, so in this type of analysis, such a binding might be revealed. If a second binding site exists, it may be present at the symmetry-related position covered by the PSI-H, -I, -B, and -G subunits. Further work is needed to clarify this point.

Origin of the LHCII Bound to PSI. Our results show that solubilization of state 2 membranes results in slightly lower numbers of PSII−LHCII supercomplexes with four bound LHCII complexes and somewhat higher numbers of supercomplexes with three bound LHCII complexes (Table 1). This suggests that among the LHCII complexes that move from the grana to PSI there are at least some that originate from the so-called M-LHCII, the LHCII that is bound to the PSII core dimer at the site of the CP29 and CP24 units (*14*). It is however hard to make quantitative statements on the origin of the LHCII that migrates to PSI. It is possible that some LHCII arises from supercomplexes that were completely disintegrated during the state transition, because the remaining complexes are too small to be picked up by our EM analysis. It is also possible that a considerable part of the migrating LHCII originates from LHCII-only parts of the grana (*28*).

In conclusion, our data show that there is a specific supercomplex of PSI−LHCII that is more abundant in state 2 than in state 1 conditions, in which the bound LHCII is

trimeric. If the binding of LHCII to PSI was not specific, the final image (Figure 5) would have been more blurred, or there would have been more than one class of projections with differences in the LHCII area. A recent suggestion that LHCII monomers can bind to the PSI complex was based on a study of the much larger PSI complex from *Chlamydomonas* (*30*). This PSI complex plus its antenna proteins, however, differs substantially form the one of green plants. But it remains possible that the group of "blurred" PSI particles (Figure 4E) we obtained predominantly in state 1 (Table 1) could contain some particles consisting of PSI and monomeric LHCII. For the set of particles from the state 2 membranes, it is clear that there cannot be many of such particles since the "blurred" particles only comprised 9%.

We note that the final resolution of the PSI−LHCII supercomplex at 16 Å was obtained even without any particular purification of the supercomplex. The binding of LHCII to PSI is probably rather weak, which is physiologically relevant to allow unbinding of LHCII and the transition to state 1. The assignment of interacting subunits was possible by comparing our medium-resolution EM data with high-resolution X-ray structures of the components. Such a hybrid EM−X-ray structural approach is very useful, as shown before for a number of complexes. Our results, however, show for the first time that an unequivocal assignment of large transient membrane-bound structure is possible even in the absence of any purification step. This stresses the potential of single-particle electron microscopy to identify such transient complexes in other types of subcellular membranes.

ACKNOWLEDGMENT

We would like to thank Dr. G. T. Oostergetel and Dr. W. Keegstra for general support and discussion.

REFERENCES

1. Allen, J. F., and Forsberg, J. (2001) Molecular recognition in thylakoid structure and function, *Trends Plant Sci. 6*, 317−326.
2. Haldrup, A., Jensen, P. E., Lunde, C., and Scheller, H. V. (2001) Balance of power: a view of the mechanism of photosynthetic state transitions, *Trends Plant Sci. 6*, 301−305.
3. Wollman, F. A. (2001) State transitions reveal the dynamics and flexibility of the photosynthetic apparatus, *EMBO J. 20*, 3623−3630.
4. Vener, A. V., van Kan, P. J., Rich, P. R., Ohad, I., and Andersson, B. (1997) Plastoquinol at the quinol oxidation site of reduced cytochrome bf mediates signal transduction between light and protein phosphorylation: thylakoid protein kinase deactivation by a single-turnover flash, *Proc. Natl. Acad. Sci. U.S.A. 94*, 1585−1590.
5. Zito, F., Finazzi, G., Delosme, R., Nitschke, W., Picot, D., and Wollman, F. A. (1999) The Qo site of cytochrome b(6)f complexes controls the activation of the LHCII kinase, *EMBO J. 8*, 2961−2969.
6. Jansson, S., Pichersky, E., Bassi, R., Green, B. R., Ikeuchi, M., Melis, A., Simpson, D. J., Spangfort, M., Staehelin, L. A., and Thornber, J. P. (1992) A nomenclature for the genes encoding the chlorophyll *a*/*b*-binding proteins of higher plants, *Plant Mol. Biol. Rep. 10*, 242−253.
7. Snyders, S., and Kohorn, B. D. (1999) TAKs, thylakoid membrane protein kinases associated with energy transduction, *J. Biol. Chem. 274*, 9137−9140.
8. Snyders, S., and Kohorn, B. D. (2001) Disruption of thylakoid-associated kinase 1 leads to alteration of light harvesting in *Arabidopsis*, *J. Biol. Chem. 276*, 32169−32176.
9. Depège, N., Bellafiore, S., and Rochaix, J. D. (2003) Role of chloroplast protein kinase Stt7 in LHCII phosphorylation and state transition in *Chlamydomonas*, *Science 299*, 1572−1575.
10. Bellafiore, S., Barneche, F., Peltier, G., and Rochaix, J. D. (2005) State transitions and light adaptation require chloroplast thylakoid protein kinase STN7, *Nature 433*, 892−895.
11. Lunde, C., Jensen, P. E., Haldrup, A., Knoetzel, J., and Scheller, H. V. (2000) The PSI-H subunit of photosystem I is essential for state transitions in plant photosynthesis, *Nature 408*, 613−615.
12. Jensen, P. E., Haldrup, A., Zhang, S., and Scheller, H. V. (2004) The PSI-O subunit of plant photosystem I is involved in balancing the excitation pressure between the two photosystems, *J. Biol. Chem. 279*, 24212−24217.
13. Zhang, S., and Scheller, H. V. (2004) Light-harvesting complex II binds to several small subunits of photosystem I, *J. Biol. Chem. 279*, 3180−3187.
14. Dekker, J. P., and Boekema, E. J. (2005) Supramolecular organization of thylakoid membrane proteins in green plants, *Biochim. Biophys. Acta 1706*, 12−39.
15. Boekema, E. J., van Roon, H., and Dekker, J. P. (1998) Specific association of photosystem II and light-harvesting complex II in partially solubilized photosystem II membranes, *FEBS Lett. 424*, 95−99.
16. Haldrup, A., Naver, H., and Scheller, H. V. (1999) The interaction between plastocyanin and photosystem I is inefficient in transgenic *Arabidopsis* plants lacking the PSI-N subunit of photosystem I, *Plant J. 17*, 689−698.
17. Lichtenhaler, H. K. (1987) Chlorophylls and carotenoids−pigments of photosynthetic biomembranes, in *Methods in Enzymology 148* (Colowick, S. P., and Kaplan, N. O., Eds.) pp 350−382, Academic Press, San Diego, New York, Berkeley, Boston, London, Sydney, Tokyo, and Toronto.
18. Penczek, P. Radermacher, M., and Frank, J. (1992) Three-dimensional reconstruction of single particles embedded in ice, *Ultramicroscopy 40*, 33−53.
19. van Heel, M., Gowen, B., Matadeen, R., Orlova, E. V., Finn, R., Pape, T., Cohen, D., Stark, H., Schmidt, R., Schatz, M., and Patwardhan, A. (2000) Single-particle electron cryo-microscopy: towards atomic resolution, *Q. Rev. Biophys. 33*, 307−369.
20. van Heel, M. (1987) Similarity measures between images, *Ultramicroscopy 21*, 95−100.
21. Boekema, E. J., Jensen, P. E., Schlodder, E., van Breemen, J. F. L., van Roon, H., Scheller, H. V., and Dekker, J. P. (2001) Green plant photosystem I binds light-harvesting complex I on one side of the complex, *Biochemistry 40*, 1029−1036.
22. Boekema, E. J., van Roon, H., Calkoen, F., Bassi, R., and Dekker, J. P. (1999) Multiple types of association of photosystem II and its light-harvesting antenna in partially solubilized photosystem II membranes, *Biochemistry 38*, 2233−2239.
23. Yakushevska, A. E., Jensen, P. E., Keegstra, W., van Roon, H., Scheller, H. V., Boekema, E. J., and Dekker, J. P. (2001) Supermolecular organization of photosystem II and its associated light-harvesting antenna in *Arabidopsis thaliana*, *Eur. J. Biochem. 268*, 6020−6028.
24. Ben-Shem, A., Frolow, F., and Nelson, N. (2003) Crystal structure of plant photosystem I, *Nature 426*, 630−635.
25. Liu, Z., Yan, H., Wang, K., Kuang, T., Zhang, J., Gui, L., An, X., and Chang, W. (2004) Crystal structure of spinach major light-harvesting complex at 2.72 Å resolution, *Nature 428*, 287−292.
26. Standfuss, J., Terwisscha van Scheltinga, A., Lamborghini, M., and Kühlbrandt, W. (2005) Mechanisms of photoprotection and nonphotochemical quenching in pea light-harvesting complex at 2.5 Å resolution, *EMBO J. 24*, 919−928.
27. Ludtke, S. J., Baldwin, P. R., and Chiu, W. (1999) EMAN: semiautomated software for high-resolution single-particle reconstructions, *J. Struct. Biol. 128*, 82−97.
28. . Jensen, P. E., Gilpin, M., Knoetzel, J., and Scheller, H. V. (2000) The PSI-K subunit of photosystem I is involved in the interaction between light-harvesting complex I and the photosystem I reaction center core, *J. Biol. Chem. 275*, 24701−24708.
29. . Boekema, E. J., van Breemen, J. F. L., van Roon, H., and Dekker, J. P. (2000) Arrangement of photosystem II supercomplexes in crystalline macrodomains within the thylakoid membrane of green plant chloroplasts, *J. Mol. Biol. 301*, 1123−1133.
30. Germano, M., Yakushevska, A. E., Keegstra, W., van Gorkom, H. J., Dekker, J. P., and Boekema, E. J. (2002) Supramolecular organization of photosystem I and light-harvesting complex I in *Chlamydomonas reinhardti*i, *FEBS Lett. 525*, 121−125.

BI051097A